Vacuum ultraviolet-absorption spectroscopy and delocalized plasma-induced emission used for the species detection in a down-stream soft-etch plasma reactor

Robert Soriano, Gilles Cunge, Nader Sadeghi

Vacuum ultraviolet-absorption spectroscopy and delocalized plasma-induced emission used for the species detection in a down-stream soft-etch plasma reactor

Robert Soriano, Gilles Cunge

JVST A
Journal of Vacuum Science & Technology A

Vacuum ultraviolet-absorption spectroscopy and delocalized plasma-induced emission used for the species detection in a down-stream soft-etch plasma reactor

Cite as: J. Vac. Sci. Technol. A **38**, 043002 (2020); https://doi.org/10.1116/6.0000134
Submitted: 21 February 2020 . Accepted: 13 May 2020 . Published Online: 04 June 2020

Robert Soriano, Gilles Cunge, and Nader Sadeghi

JVST A
Journal of Vacuum Science & Technology A

ARTICLE

avs.scitation.org/journal/jva

Vacuum ultraviolet-absorption spectroscopy and delocalized plasma-induced emission used for the species detection in a down-stream soft-etch plasma reactor

Cite as: J. Vac. Sci. Technol. A 38, 043002 (2020); doi: 10.1116/6.0000134
Submitted: 21 February 2020 · Accepted: 13 May 2020 ·
Published Online: 4 June 2020

Robert Soriano, Gilles Cunge,[a] and Nader Sadeghi

AFFILIATIONS

Laboratoire des Technologies de la Microélectronique, Univ. Grenoble-Alpes, CNRS, CEA/LETI Minatech, Grenoble, France

Note: This paper is part of the Special Topic Collection Commemorating the Career of John Coburn.
[a]**Electronic mail:** gilles.cunge@cea.fr

ABSTRACT

Vacuum ultraviolet-absorption spectroscopy (AS) and emission spectroscopy (ES) from delocalized probe plasma are implemented in the downstream chamber of a soft-etch industrial plasma reactor. A capacitively coupled plasma plasma, running in the upper compartment in $He/NF_3/NH_3/H_2$ mixtures at about 1 Torr, produces reactive species which flow through a shower head into a downstream chamber, where they can etch different μ-electronic materials: Si, SiO_2, SiN, etc. The ES reveals the presence of F atoms, while the dissociation rates of NF_3 and NH_3 are deduced from the AS, as well as the density of HF molecules, produced by chemical chain-reactions between dissociation products of NF_3, NH_3, and H_2. The variations of HF density as a function of the NH_3 flow rate suggest the possible formation of NH_4F molecules in the plasma.

I. INTRODUCTION

Downstream etchers known as remote plasma sources (RPS) were introduced in the early 1970s for resist stripping applications.[1,2] However, until recently, they have drawn relatively little scientific interest compared to other plasma sources because they inevitably lead to isotropic etching, which restrict their use to specific applications. But as the size and thickness of transistors continue to shrink, new processes are required to etch high aspect ratio (AR) nanofeatures. For example, ultrahigh selective isotropic etching in RPS is needed for specific steps involved in the patterning of FinFet[3] transistors and 3D Nand memories.[4] RPS processes have also started to be investigated[5] to replace wet processes that show severe limitation to remove materials in AR structures due to capillary forces. Finally, plasma induced damage (mostly caused by energetic ions and photons) has become a major concern and new etching technologies (involving RPS in combination with typical plasmas) such as the Smart Etch[6] and other ALE processes[7] have been introduced to etch materials anisotropically without damages. As a matter of fact, the interest of RPS lies in their capabilities to produce purely chemical etching with radicals leading to high selectivity and absence of structural damages in underlayers.

In many of the above mentioned applications, the goal is to etch selectively an Si alloy, respectively, to another Si alloy (e.g., Si, SiN, and SiO_2), which can be achieved in F-based RPS plasmas. NF_3 is typically used as an F source due to its high cross section for dissociative electron attachment.[8] Furthermore, F atom's density in the discharge can be controlled by adding H or O containing gases into NF_3. For example, downstream plasmas in NF_3/O_2 mixtures have been used to etch selectively SiN to SiO_2,[9] and remarkable performances were obtained recently[4] to remove SiN from trenches with AR of 100, thus performing better than in wet processes.

On the other hand, H addition to NF_3 in RPS (which are studied in this paper) leads to new etching possibilities. Initially, such processes were introduced[10] to deoxidize silicon surfaces, i.e., etch SiO_2 selectively to Si prior to epitaxy, or to clean shallow trench isolation (STI) trenches. These processes were achieved in

NF_3/H_2 (Refs. 11 and 12) or NF_3/NH_3 chemistry.[13] The addition of hydrogen to NF_3 does not only serves to reduce F atoms density but also to promote the formation of new radicals such as HF or NH_4F, which are believed to be the precursor to the formation of ammonium salts $(NH_4)_2SiF_6$ selectively on SiON and SiOx surfaces.[14–16] In this case, there is no direct etching of the surface during the RPS step: the salt forms selectively with a material to be etched and must then be sublimated to readily etch the material. Several innovative etching processes have been developed recently based on this phenomenon, including the so-called Smart Etch process6 and several atomic layer Etching processes[7,17] all of which are two step processes: the material is first modified anisotropically on a well-controlled depth by a given plasma and the modified layer is then etched selectively in a second step, typically by an RPS in NF_3/NH_3 chemistry. The "Smart Etch" process is using energetic H_2 or He ions generated in a capacitively coupled plasma (CCP) plasma for the first step, thus modifying several nm of the SiN material by ion implantation (the use of light ions prevents SiN sputtering),[18,19] Initially, the modified SiN* layer was removed selectively to pristine SiN by a wet HF[6] or by gaseous HF.[20] But this does not allow cycling the two step of the process with a good throughput. By contrast, by removing the modified SiN* layer with an RPS in NF_3/NH_3 mixtures,[21] it becomes possible to perform the implantation and RPS steps without air exposure in the same specifically design chamber.[22] For industrial applications, the salt formed during the RPS step is sublimated either by heating,[17] or simply by reducing the pressure before the next implantation step.[22] Recent work[22] has demonstrated that $(NH_4)_2SiF_6$ salt formation is efficient only on oxidized surfaces, explaining the SiO_2/Si and SiO_x/SiN etching selectivity as well as the SiN*/SiN selectivity in the Smart Etch process: in the H_2 or He plasma used to modify the SiN there is a considerable amount of O implantation in the SiN* originating from plasma impurities. Interestingly, while the salt formation has been widely analyzed through surface diagnostics, the origin of radicals that are precursors to their formation remains highly speculative; since the gas phase of NH_3/NF_3 RPS has never been analyzed. The consensual[10,15,21–24] mechanism for the salt formation in this chemistry is described by the following stochiometric balance (real reactions at the wafer being probably the result of a long series of individual mechanistic steps),

$$SiO_2 + 2NH_4F + 4HF \rightarrow (NH_4)^2SiF_6 + 2H_2O. \quad (1)$$

Therefore, NH_4F, HF, and $NH_4F(HF)$ are typically assumed to be formed in the plasma and hence they react with the surface. As a matter of fact, the work from Ogawa[15] indirectly suggests that NH_4F could be produced from the reaction of NH_3 gas with some fragment of NF_3 (formed by heating NF_3). The formation of HF in the plasma can also be expected to play a significant role in the overall chemistry and we can expect HF to be formed by the chain reactions (2–4) (well known in HF laser physics):[25–30]

$$H_2 + F \rightarrow HF + H, \quad (2)$$

$$H + NF_X(x = 1, 2) \rightarrow HF + NF_{x-1}, \quad (3)$$

$$NH_3 + F \rightarrow NH_2 + HF. \quad (4)$$

In the present paper, we apply the vacuum ultraviolet broadband absorption spectroscopy (VUV-BBAS) in the 120–200 nm range[31,32] with a deuterium lamp as the light source for the real time monitoring of etching agents and etch products in the downstream of NF_3–NH_3–H_2 containing plasmas of an AMAT RPS reactor especially designed to perform Smart Etching and described in detail in Ref. 22. Besides VUV-BBAS, we also have implemented a probe pulsed DC discharge to follow, by actinometry, the density of F atoms in the downstream chamber. By directly measuring the densities of NH_3, NF_3, and HF, as well as the variation of F density as a function of the operating condition, we could get insights into the complex chemistry of these RPS plasmas.

II. EXPERIMENT

A. Plasma reactor

The experiments are carried out in an industrial 50 cm diameter remote plasma reactor (*frontiers* from Applied Materials) used for the soft etching of 30 cm diameter wafers. It is composed of two chambers separated by an about 50 mm thick shower head. As shown in Fig. 1, the gas, whose main component is helium and contains a few percent of H_2, NF_3, and NH_3, enters the top compartment, flows through the shower head to expand into the downstream compartment and is then pumped out with a 200 l/s dry primary pump. The total gas flow rate is about 2000 SCCM and the gas pressure in the downstream chamber (DSC), measured with a capacitance gauge, is maintained to 1 Torr with a throttle valve located on the pumping pipe. A capacitively coupled plasma (CCP) is generated in the top compartment with up to 500 W power of 13.56 MHz radiofrequency discharge. Radicals and atoms produced by the discharge are transported by the gas flow into the *DSC* but the plasma production zone is limited by the shower head, blocking the extension of the discharge into the downstream compartment. Thus, only radicals are responsible for the soft etching of the wafer

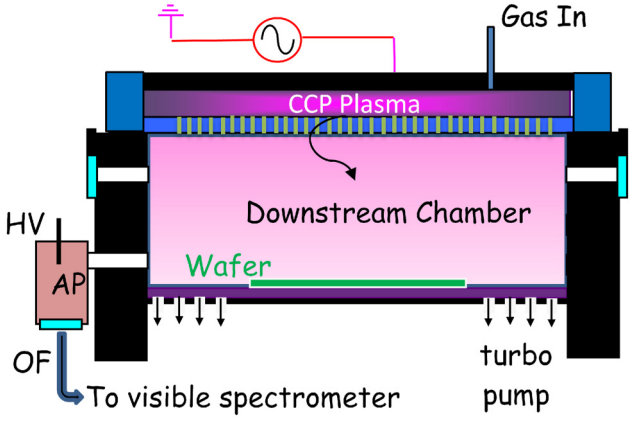

FIG. 1. Schematic of the experimental setup showing the downstream chamber with the small deported plasma (used for OES).

positioned in the *DSC*, without any assistance by ion bombardment, as is the case in usual reactive ion etching processes.[33] Due to the absence of viewports in the *CCP* zone of the reactor, no diagnostic technique can be implemented to characterize the *CCP* plasma. However, atoms and molecules produced by the dissociation of injected molecules in this plasma and transported to the *DSC* have been monitored in this chamber by the vacuum ultraviolet broad-band absorption spectroscopy (VUV-BBAS) and by optical emission spectroscopy (OES). But, as a consequence of the absence of energetic electrons in the downstream plasma, no optical radiation is emitted from this region. Thus, to monitor the density of F atoms present in the downstream chamber, a small tube (about 4 cm inner diameter, 10 cm long) is connected to the *DSC* through a 4 cm diameter hole on the reactors' wall and an auxiliary plasma (AP) is generated inside this tube by applying a positive high voltage (HV) to an isolated, 0.2 cm diameter, 3 cm long copper road which penetrates into the tube by one of its end, as shown in Fig. 1. The opposite end of the tube is sealed by a quartz window for the *OES* and the inner walls of the tube act as a cathode for the auxiliary discharge.

B. Actinometry with auxiliary plasma

To follow the variation of F atoms densities produced by the *CCP* discharge, the optical emission of the auxiliary discharge is collected by an optical fiber, whose other end is set on the entrance slit of a 50 cm focal length monochromator (Acton 500 i), equipped with a 600 groves/mm grating and backed by a 1024 elements, 25 μm pitch photodiode array. A 112 kΩ resistor, placed in series with the *HV* supplier, limits the peak discharge current of the *AP* to about 8 mA with a 1 kV applied voltage. And moreover, the HV is modulated at 120 Hz, with a 5% duty cycle to keep as low as possible the dissociation of the gas inside the auxiliary discharge tube. Thus, we assume that the recorded emission intensities from the excited states of F and He atoms, at 703.7 and 706.5 nm lines, respectively, are proportional to the densities of these atoms in the downstream chamber. The actinometry method,[34,35] with 706.5 nm helium line for the reference intensity, is used to follow changes on F atoms' densities when varying the amount of the added gases to helium. We are aware that the large difference between the excitation energies of helium line (22.7 eV) and that of F line (14.7 eV) render questionable the use of helium as the actinometer gas.[34] But we consider that with helium remaining the main component of the feed gas, the electron temperature in the auxiliary plasma should not significantly change with the variation of the minor components, which are H_2, NF_3, NH_3, and radicals produced by their dissociation in the CCP plasma. Thus, assuming constant excitation cross section of species and neglecting the quenching of excited states by the gas, we apply the simplified actinometry equations:[35,36]

$$I_{706} = G \cdot K_{706} \cdot n_e \cdot [\mathrm{He}], \tag{5}$$

$$I_F = G \cdot n_e \cdot (K_F \cdot [\mathrm{F}] + K_{PF} \cdot [\mathrm{NF_3}]), \tag{6}$$

where G is a geometric factor, [He] and [F] are the densities of helium and F atoms, with I_{706} and I_F being their respective recorded intensities and [NF_3] is the remaining density of NF_3 molecule in the *AP*, whose dissociative excitation can contribute to the production of F atom in the upper state of the 703.7 nm line, with K_F being the corresponding rate coefficient. To write (6), the contribution to the I_F intensity of the other dissociation products of the gas in the CCP, excepted F atoms, is neglected. The excitation coefficient K_{PF} of the precursor molecule is deduced by measuring I_F when known amount of the NF_3, diluted in helium, is introduced into the reactor in the absence of the CCP discharge. And, as will be described in the following section, the density of precursor molecules NF_3 in the downstream chamber, thus in the auxiliary plasma, can be measured by the *VUV-BBAS*. Hence, the contribution of *NF_3 molecules* to the I_F can be evaluated and subtracted for obtaining I_F^c, the intensity originated from the sole direct excitation of the ground state F atoms in the auxiliary plasma. And finally, the variation of the density of *F* atoms in the downstream chamber, when changing the gas mixture and *CCP* discharge conditions, can be followed by using the simplified equation:

$$[\mathrm{F}] \sim [\mathrm{He}] \frac{I_F^c}{I_{706}}. \tag{7}$$

C. Broad-band absorption spectroscopy

The absolute densities of NH_3 and NF_3 molecules in the downstream chamber, thus their dissociation rates in the CCP chamber, as well as the density of HF molecules formed from the dissociation products, have been measured by the broadband absorption technique.[31,37,38] A schematic of the top view of the reactor, with the VUV-BBAS setup is shown in Fig. 2. Shortly, the light source is a high-pressure deuterium (D_2) lamp (X2D2 from Hamamatsu) that emits a continuum radiation down to 120 nm. A VUV grade parabolic mirror produces a collimated, 1 cm diameter, light beam at 90° from the incident light. This VUV beam crosses the downstream chamber, through two optical ports facing each other and equipped with MgF_2 windows, at about 5 cm below the

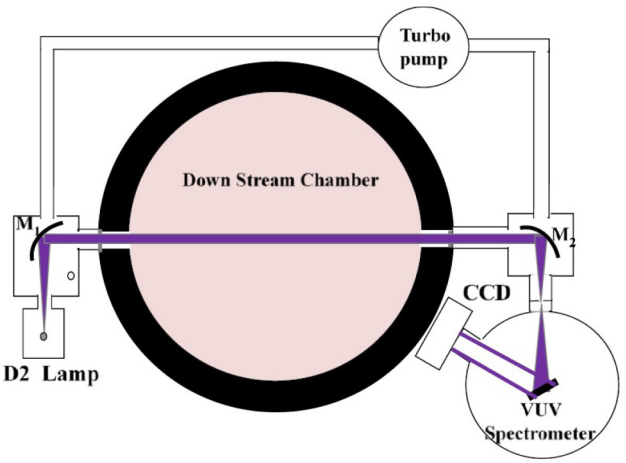

FIG. 2. Top view of the reactor showing the VUVAS experiment with the D2 light source and the VUV monochromator equipped with the CCD camera.

shower head (see Fig. 1). At the exit of the second window, another VUV grade parabolic mirror focuses the VUV beam onto the entrance slit of a 20 cm focal length VUV spectrometer (Jobin-Yvon H20-UVL), equipped with a 1200 groove/mm concave VUV grating. The exit port of the spectrometer was modified to accept a VUV CCD camera (Newton DO940 for X-ray and VUV from Andor) with 2048×512 pixels of 13.5 μm pitch size. In the central part of the CCD (between pixels 600–1500), the linear dispersion is 0.047 nm/pixel and the ultimate spectral resolution of the system is about 0.14 nm with a 20 μm entrance slit width. But, the spectral resolution is degraded in the edges of the CCD. Turbomolecular pumps maintain a background pressure below 10^{-4} Torr in the entire optical path of the VUV light outside the reactor chamber (D_2 lamp to the reactor input window and the exit window to the CCD). As usual in *BBAS* experiments,[38] the absorption spectra of the gas in the downstream chamber are obtained by recording three spectra with the CCD: (i) the background with the lamp off (*BG*), (ii) the emission of the lamp without the gas flow, L_0, and (iii) the transmitted light of the lamp [$I_P(\lambda)$] with the gas flow On. We underline that the absence of energetic electrons in the *DSC* results in the absence of plasma emission, which can be neglected. The absorbance spectra (A_λ), which is related to the wavelength dependent absorption cross-section $\sigma(\lambda)$ of the molecules through the Beer–Lambert law, is obtained by

$$[A]_\lambda = \mathrm{Ln}\left(\frac{I_0(\lambda)}{I_T(\lambda)}\right) = \mathrm{Ln}\left(\frac{L_0(\lambda) - BG}{I_P(\lambda) - BG}\right) = \sum_i \sigma_i(\lambda) l N_i, \qquad (8)$$

where I_0 and I_T are the intensity of the incoming and transmitted VUV light, index "i" refers to different absorbing species present in the chamber with density N_i, and l is the absorption length. Although the absorption cross sections of NH_3 (Refs. 39–42) and NF_3 (Refs. 43–45) have been reported in the literature, for the determination of their partial pressures in the downstream chamber, we have used our own collection of absorbance spectra recorded when the reactor was filled with these gases at different known pressures in the absence of discharge. This collection of spectra constitutes some sort of reference tables. As an example, recorded absorbance spectra of NH_3 and NF_3 are reported in Figs. 3 and 4 for a few indicated pressures. This way of proceeding has the advantage of being insensitive to changes on the spectral profile of NH_3 with the spectral resolution of the spectrograph + CCD. Opposite to the NF_3 case, for which the VUV photon absorption ends up in a predissociated continuum, the upper states of the VUV transitions in NH_3 are Rydberg states, with vibrational and rotational levels. In Fig. 3, transitions to these electronic states and corresponding vibrational levels are identified, but the rotational structure cannot be resolved. The absorption profile is thus composed of many narrow ro-vibrational transitions and important modifications on the behavior of the absorbance curves can be observed with the spectral resolution of the detection system (compare spectra in Refs. 40 and 42). It should be pointed out that the entrance slit of the spectrometer was kept unchanged and consequently, the spectral resolution was identical in all spectra recorded in plasma conditions and for the abacus. Also, using the calibration spectra of the abacus for the determination of NH_3 partial pressure under plasma conditions eliminates a possible error source by the saturation of the peak absorbancies.[39]

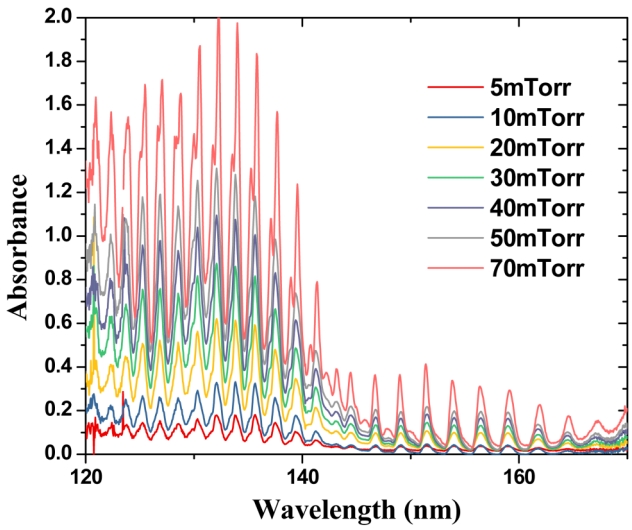

FIG. 3. VUV absorption spectrum of NH_3 gas (no plasma) at several reactor filling pressures.

III. RESULTS AND DISCUSSION

A. Characterization of HF spectrum

Dissociation of NF_3 in CCP plasma produces F atoms that can rapidly react with H containing molecules to form HF molecules.[26,28] Strong absorption spectra of HF in the VUV spectral range have

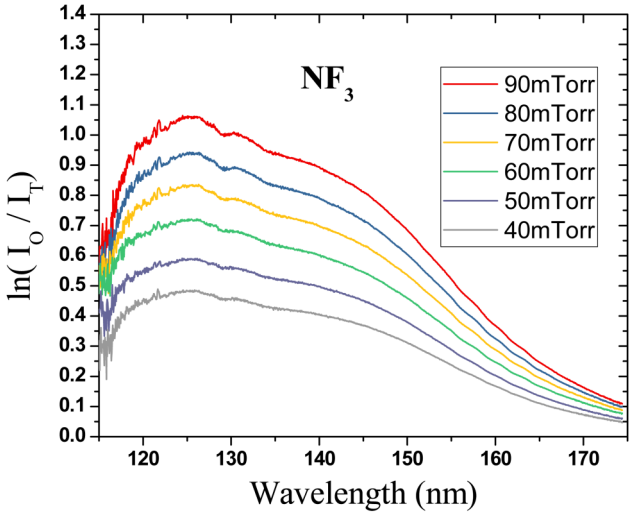

FIG. 4. VUV absorption spectrum of NF_3 gas (no plasma) at several reactor filling pressures.

been reported in the literature[46,47] and its detection by VUV-BBAS was thus highly expected. The experiments have been carried out in the afterglow of NF_3/H_2 mixture in which HF is produced by the reaction of F atoms resulting from the plasma dissociation of NF_3 with H_2 molecules [reaction (2)], for which a rate coefficient $k_2 = 2-3 \times 10^{-17}$ $m^3 s^{-1}$ has been reported.[26,28] Absorption spectra recorded in the downstream chamber without and with a discharge in the CCP chamber are shown in Fig. 5. The experimental steps are:

A mixture of 4% NF_3/9% H_2 diluted in helium is flown through the reactor and the exit throttle vale is adjusted for obtaining 1 Torr total pressure in the downstream chamber.

The recorded VUV spectra are identical to the one obtained at 40 mTorr of NF_3 from the abacus of Fig. 4. As NF_3 does not react with H_2, we conclude that the partial pressure of NF_3 in the *DSC* is 40 mT in the absence of plasma.

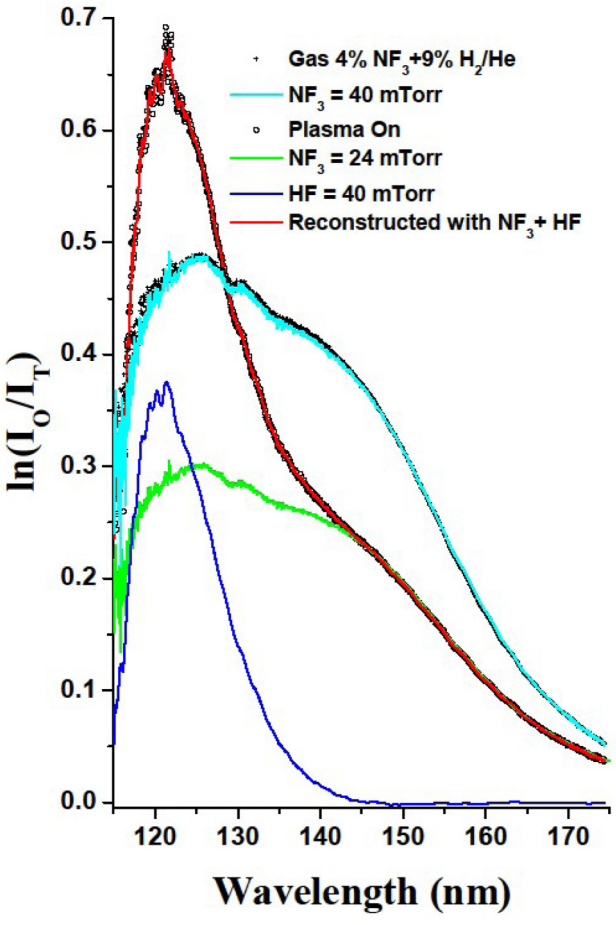

FIG. 5. Black cross (+): absorption spectra recorded in an NF_3 (4%)/H_2 (9%)/He gas and adjusted with a pure NF_3 spectrum recorded at 40 mTorr (cyan line). Black open circle (°): absorption spectrum recorded with the plasma ON (250 W). This spectrum can be fitted in its high wavelength part by the green curve, which corresponds to NF_3 gas at 24 mTorr. By subtracting this NF_3 contribution to the overall spectrum, we obtain the VUV absorption spectrum of HF molecules (blue line), corresponding to a pressure of 40 mTorr HF according to its absorption cross section.

A 250 W plasma is stuck in the CCP compartment and after a few seconds of stabilization time, a new VUV absorption spectrum is recorded. As seen in Fig. 5, the shape of this new spectrum is totally different from the previously recorded in the absence of CCP plasma. This modification revels absorption by new species formed under the CCP plasma action, which, as previously discussed, is an HF molecule. However, the high wavelength tail of the new spectrum can be fitted by the absorption spectrum of NF_3 at a pressure of 24 mTorr, indicating that about the half of the NF_3 molecules was dissociated by the CCP plasma. The new spectrum, obtained when subtracting the absorption curve of 24 mTorr NF_3 from the recorded spectra with the plasma ON, corresponds to the $A^1\Pi \leftarrow X^1\Sigma^+$ absorption spectrum of HF molecules. This attribution is justified by the similarity of this spectrum with the one obtained by Nee *et al.* from synchrotron radiation absorption by HF gas.[46] These authors also provide the wavelength dependent absorption cross section, from which the absorbance can be converted into the density of HF in the DSC by using Eq. (8). The deduced partial pressure of HF in the example presented in Fig. 5 is 40 mTorr. Given that $A^1\Pi$ state is predissociated, because its energy is above the D°=5.87 eV dissociation limit of HF,[48] the HF($A^1\Pi \leftarrow X^1\Sigma^+$) absorption spectrum is a continuum, with its absorbance being scaled with the HF density, for a fixed absorption length. We will thus use in the following the absorbance spectrum deduced from NF_3/H_2 plasma, depicted in Fig. 5, for the determination of the amount of HF molecules produced in other plasma conditions.

As an example, in Fig. 6 are shown absorption spectra recorded in the downstream chamber without and with CCP plasma in 1.6% NF_3/2% NH_3 diluted in helium gas at a total flow rate of 2 l/min and 1 Torr pressure in the DSC. The spectrum recorded in the absence of CCP plasma results from absorption by only NF_3 and NH_3 and can be reconstructed by adding absorbance spectra from 16 mTorr of NF_3 and 20 mTorr of NH_3, which indicates their partial pressures in the DSC. Striking a 350 W, CCP plasma results in an important diminution of the partial pressures of NF_3 and NH_3, which are highly dissociated by the discharge, and hence in weaker absorbance. The new absorption spectra with the CCP plasma ON can be reconstructed by adding absorbance spectra of 7.7 mT of NF_3, 4 mT of NH_3, and 20 mT of HF. Thus, about 50% of NF_3 and 80% of NH_3 of the introduced gas have been dissociated by the plasma and, as will be discussed in following sections, the chain reactions of the dissociation products lead to the formation of HF molecules.

The partial pressures of NF_3, NH_3, and HF in all gas mixtures and plasma conditions have been deduced like in Fig. 6, by the best adjustment of the recorded absorption spectrum with the sum of three absorbance curves of these molecules with adequate amplitudes. Considering the reproducibility of results from several experiments, the uncertainty on determined partial pressures is estimated to be about 7% of the evaluated values plus 1 mTorr.

B. Kinetics of NF_3/H_2 plasmas

Dissociation of NF_3 in the CCP plasma produces also NF_2 and NF radicals that rapidly react with H atoms, produced by the

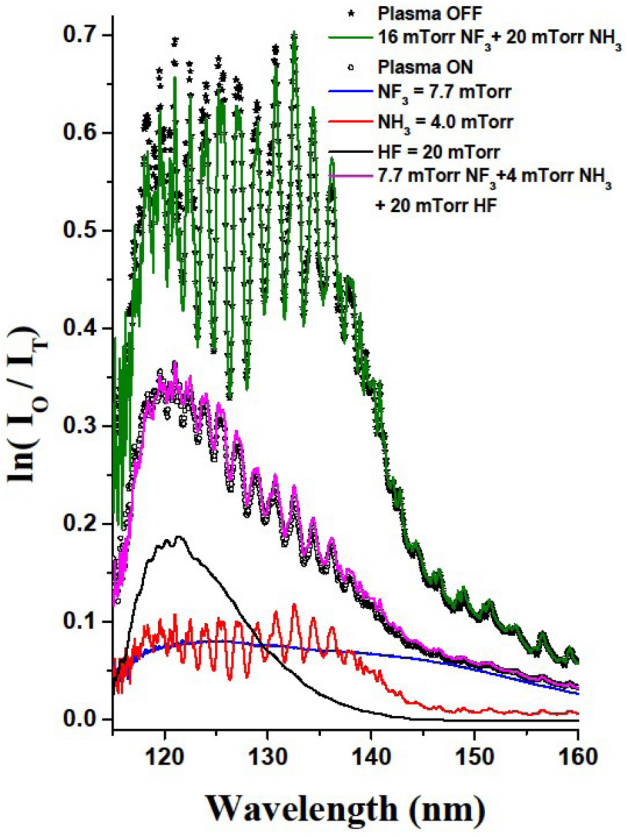

FIG. 6. Black aster (*): absorption spectra recorded in an NF_3/NH_3/He gas mixture gas/He gas and adjusted (green line) with the spectra from the abaques with the sum of 16 mTorr of NF_3 and 20 mTorr of NH_3. Black open circle: absorption spectrum recorded with the plasma ON (250 W). This spectrum can be fitted by the sum of three spectra: HF (20 mTorr), NF3 (7.7 mTorr), and NH_3 (4 mTorr).

dissociation of H_2 in the CCP, but also reaction (2). The chain reactions which follow are

$$H + NF_2 \rightarrow NF + HF, \quad (9)$$

$$H + NF \rightarrow N + HF, \quad (10)$$

$$NF + NF \rightarrow N_2 + 2F, \quad (11)$$

for which the rate coefficients reported in the literature are $k_9 = 1.9 \times 10^{-17}\ m^3\ s^{-1}$;[49] $k_{10} = 2.5 \times 10^{-17}\ m^3\ s^{-1}$ (Refs. 49 and 50), and $k_{11} = 7 \times 10^{-17}\ m^3\ s^{-1}$ (Refs. 49 and 50). These fast chain reactions, whose main final product is HF molecule, can continue as far there are enough H_2 molecules and/or CCP generated F atoms in the chamber. Figure 7 illustrates the consumption of plasma generated F atoms and production of HF in NF_3/H_2/He (100/100/1900 SCCM) gas mixture and pressure fixed at 1 Torr in the *DSC*. With increasing RF power of the CCP, the steady-state partial pressure of NF_3 in the downstream chamber drops gradually from its initial value of 52 mTorr to 20 mTorr at 350 W. Simultaneously, the partial pressure of produced HF molecules increases, reaching 90 mTorr at 350 W. It is also shown in this figure the ratio between the partial pressure of HF and the missing partial pressure of NF_3. This ratio clearly shows that three HF molecules are produced for one missing NF_3 molecule, indicating that once an NF_3 molecule starts to be dissociated, producing the first F atom, the chain reactions (2) and (9)–(11) will consume the other by-products of the dissociation (NF_2 and NF) to form HF molecules. In the above presented example, the limiting factor of the chain reactions is the amount of the plasma dissociated NF_3 molecules, which depends on RF power. Higher is the RF power, larger is the dissociation rate of NF_3 and larger is the amount of produced HF. However, the limiting factor can also be the amount of H atoms, produced by the plasma dissociation of H_2 molecules or by reaction (2), available for the chain reactions. In Fig. 8 are reported the partial pressures of NF_3 and HF in the DSC versus the amount of H_2 in the feed gas, composed of 100 SCCM of NF_3, x SCCM of H_2 and 1900 −-x SCCM of helium. The RF power in the CCP is fixed at 250 W and the total pressure in the DSC is 1 Torr. At the beginning, with increasing H_2 flow rate, the partial pressure of HF increases almost linearly to reach its maximum at about 100 SCCM of H_2, while NF_3 density remains almost constant. In fact, the dissociation rate of NF_3, thus the amount of F atoms in the DSC is fixed by the RF power in the CCP and up to 100 SCCM of H_2 the total number of F atoms resulting from the dissociation of NF_3 exceeds the double of the number of introduced H_2 molecules. Thus, every H_2 of the feed gas produces two HF molecules. This is seen from the linear increase of the ratio (HF/dissociated NF_3) during the initial phase of the H_2 flow rate rise, also shown in Fig. 8. The actinometric emission intensity of the 703.7 nm F line in the auxiliary plasma, which is indicative of the partial pressure of fluorine atoms in the

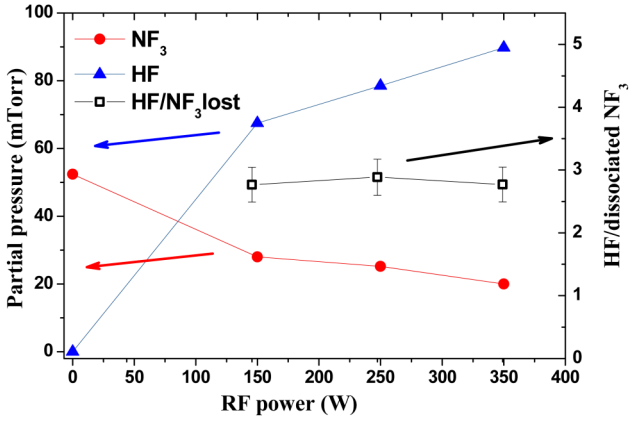

FIG. 7. Variations of the densities of HF and NF_3 as a function of the RF power in NF_3/H_2 plasmas. The hollow black squares show the ratio of the HF density divided by the density of NF_3 which is lost when the plasma is ON, indicating that each lost NF_3 leads to the formation of 3 HF molecules.

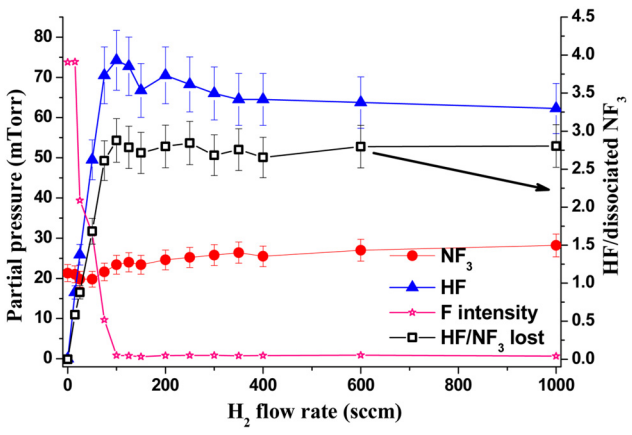

FIG. 8. Impact of the H_2 dilution in NF_3 on the densities of NF_3, HF, F, and on the ratio of produced HF per lost NF_3.

DSC, is also plotted in Fig. 8. Its behavior indicates that, as expected, the density of F atoms in the DSC decreases as the H_2 flow rate increases up to about 100 SCCM. Above this value, there are enough H_2 molecules in the reactor to consume all F atoms of the dissociated NF_3 molecules, and the intensity of the 703.7 fluorine line from the auxiliary plasma remains zero.

In conclusion, below 100 SCCM of H_2, this is the amount of H_2 molecules of the feed gas which limits the quantity of HF produced inside the reactor but above 100 SCCM, the dissociation rate of NF_3 will become the limiting factor. However, as the amount of H_2 in the feed gas becomes significant, its vibrational and rotational excitation will lead to a slight lowering of the electron temperature in the CCP plasma, resulting in a small diminution of the dissociation rate of NF_3. This is the reason for the small enhancement of the partial pressure of NF_3 after its minimum density at 100 SCCM of H_2 and the simultaneous lowering of the HF density, as seen in Fig. 8. However, the ratio of the partial pressures of HF over the dissociated NF_3 remains close to 3, attesting that any of NF_3 molecules that starts to be dissociated by losing a flour atom, is fully consumed by the chain reactions (2) and (9)–(11) to form, in the end, three HF molecules.

C. Kinetics of NF_3/NH_3 plasmas

F and H atoms produced in the CCP chamber by the dissociation of NF_3 and NH_3, trigger a series of chain reactions which leads to the production of large amount of HF molecules. In Table I are reported the measured partial pressures of NF_3, NH_3, and HF in the gas introduced into the reactor chamber (plasma off, 0 W) and for three different RF powers. The introduced gas mixture is NF_3/NH_3/He (50/50/1950 SCCM) and the pressure in the *DSC* is fixed to 1 Torr. In the absence of plasma, the partial pressures of NF_3 and NH_3 are 25 and 27 mTorr, respectively. Striking the CCP plasma in the upper chamber with 150 W RF power results in a drastic decrease (by factor 7) of the NH_3 partial pressure in the downstream chamber, whereas that of NF_3 is only divided by 2. This different behavior is opposite to an expectation based on binding energy of F atom in NF_3 (2.9 eV) and H atoms in NH_3 (4.1 eV), which should favor a higher dissociation rate of the former. But, the difference reflects the fact that electron impact is the only process responsible for the dissociation of NF_3 molecules, whereas the so produced F atoms can also react with NH_3, according to reactions (4) and (12),[10,15,51,52]

$$HF + NH_3 \rightarrow NH_4F. \quad (12)$$

Reaction (4), which is very fast with $k_4 = 1-4 \times 10^{-16}\ m^{-3}\ s^{-1}$ according to the litterature,[30] can explain why the newly generated HF molecule, with its partial pressure of 28 mTorr, becomes the most abundant molecule in the *DSC* at the lowest 150 W of CCP power.

With increasing RF power, thus increasing plasma density in the CCP chamber, NF_3 and NH_3 are more dissociated but the enhancement of their dissociated parts, also reported in columns 5 and 7 of Table I, is much slowed down. Accordingly, the amount of the produced HF increases, but it seems to levels off above 300 W RF power. We note that when RF power exceeds 150 W, due to the excess of plasma generated H atoms, all F atoms produced by the dissociation of NF_3 are converted to HF molecules.

Figure 9 shows the impact of the NH_3 dilution (for a fixed NF_3 flow rate of 50 SCCM and total flow rate of 2050 SCCM at 250 W CCP power) on the densities of NH_3, NF_3, HF, and also on the amount of NH_3 and NF_3 lost (compared to the plasma OFF). The amount of NF_3 lost is multiplied by a factor of 3 in this figure to highlight the relationship between the HF density and the amount of F produced by NF_3 dissociation (assuming that 3 F atoms are produced for each NF_3 lost, as previously observed in NF_3/H_2 plasmas). The variation of F is not shown because it drops rapidly below the detection limit as soon as 25 SCCM of NH_3 is added to NF_3. The density of NF_3, whose gas flow rate is constant at 50 SCCM, is increasing slowly with the amount of NH_3 injected in the discharge. This is attributed to the small decay of the electron temperature/density with increasing NH_3 density in the mixture, as well as with a change of its loss rate by pumping when modifying the gas mixture. Indeed, as a consequence of the molecular mass dependence of the pumping speed, the density of NF_3 without plasma (not shown) is also slightly increased when changing the NH_3 dilution from 100 to 400 SCCM. As a result, with the CCD plasma on, the amount of NF_3 lost is almost not varying for the NH_3 flow rate ranging between 100 and 400 SCCM. The density of HF rises rapidly to reach a maximum value at 50 SCCM NH_3, while at the same time, the NH_3 density remains negligibly low. This behavior is in good agreement with the results of Table I and with reaction (4): F atoms produced from NF_3 dissociation react rapidly with NH_3 to produce HF. As far there is enough F available, all the injected NH_3 molecules are consumed by reaction (4) and the HF density rises accordingly. NH_3 is fully dissociated for its flow up to approximately 50 SCCM, at which point there is no more F atoms available: the NH_3 density then increases and above 75 SCCM it raises almost linearly with the NH_3 flow rate. Surprisingly, the HF density appears to decay significantly when the NH_3 flow rate overpass about 50 SCCM: once all F atoms available are consumed by NH_3 to form HF, one would expect the HF density to reach a steady state. A fraction of this decay can be

TABLE I. Measured partial pressures of NF_3, NH_3, and HF at different RF powers of CCP, together with dissociated parts of NF_3 and NH_3 and the ratios of HF over dissociated parts.

RF power (W)	Measured NF_3 (mT)	Measured NH_3 (mT)	Measured HF (mT)	Dissociated NF_3 (mT)	HF/missing NF_3	Dissociated NH_3 (mT)	HF/missing NH_3
0	25	27	0	0		0	
150	12	4	28	13	2.2	23	1.2
250	10	3	44	15	2.9	24	1.8
350	9	1,5	48	16	3.0	25.5	1.9

attributed to the fact that less NF_3 is dissociated when the NH_3 gas flow rate is increased (as previously observed in NF_3/H_2 mixtures, Fig. 8) but this is far from being enough to explain the observed HF density decay. Indeed, the ratio NF_3loss/HF drops from about 3 at 50 SCCM NH_3 to 1.8 at 400 SCCM of NH_3, suggesting that a significant part of the HF produced is lost by a new mechanism. Furthermore, the amount of NH_3 lost would also be expected to be constant for the same reason, although it shows a significant increase with the NH_3 flow rate. As a matter of fact, there seems to be a correlation between the amount of NH_3 lost and the amount of HF decreases after its maximum at 50 SCCM of NH_3 when its flow rate increases above 75 SCCM. All these observations are strongly suggesting that reaction (12) is taking place efficiently under our conditions, i.e., that NH_3 reacts with HF to produce NH_4F, which is believed to be one of the main precursors for the formation of salts on the wafer. This reaction, which is used to produce NH_4F commercially,[53] is fully reversible. But since NH_4F is poorly volatile at low temperatures, it will then condense efficiently on cold enough surfaces to form a crystal. Furthermore, at one Torr pressure, three body recombination reactions can proceed at high enough rates (especially between large size molecules, which can share the excess energy of the reaction between a large number of available bonds). It is thus reasonable to assume that reaction (12) producing NH_4F take place under our experimental conditions, even if this remains speculative since NH_4F is not directly observed. Thus, the NH_4F density can be roughly estimated from the loss of HF (accounting for the reduced NF_3 loss) or directly from the loss of NH_3, as shown in Fig. 10. We observe a qualitative agreement between the two estimations, although a significant quantitative divergence is observed at high NH_3 dilution, where the NH_4F density deduced from NH_3 loss is significantly larger (more than a factor of two) than that deduced from HF decrease. This is probably due to the assumption that the NH_3 loss is caused solely by reactions with HF: the NH_3 density is actually driven by several processes, including, for example, the recombination $NH_2+H \rightarrow NH_3$, which depend on the H density and thus on the H atoms recombination rate on the reactor walls to form H_2 (which may be plasma chemistry dependent). Nevertheless, our results are suggesting that significant amount of NH_4F is produced in the discharge at large NH_3 dilutions, i.e., the processing conditions used to form salts on the wafer in industrial etching processes.[22]

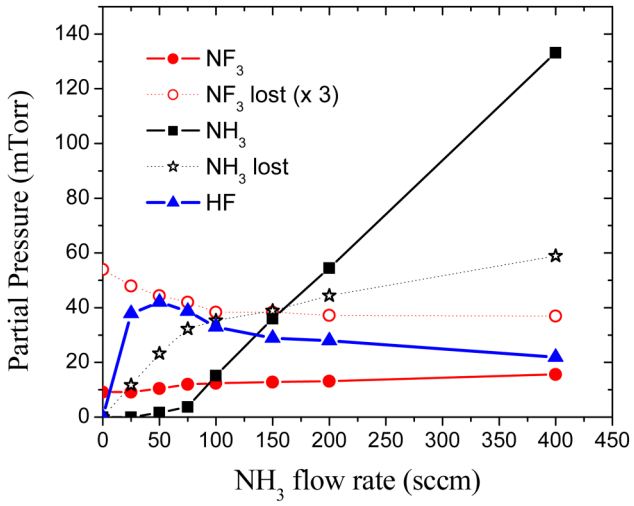

FIG. 9. Impact of the NH_3 flow rate in He/NF_3 (50 SCCM flow rate) plasma on the densities of NF_3, NH_3, HF and on the amount of the lost NH_3 and NF_3 when the plasma is ON with a 250 W RF power.

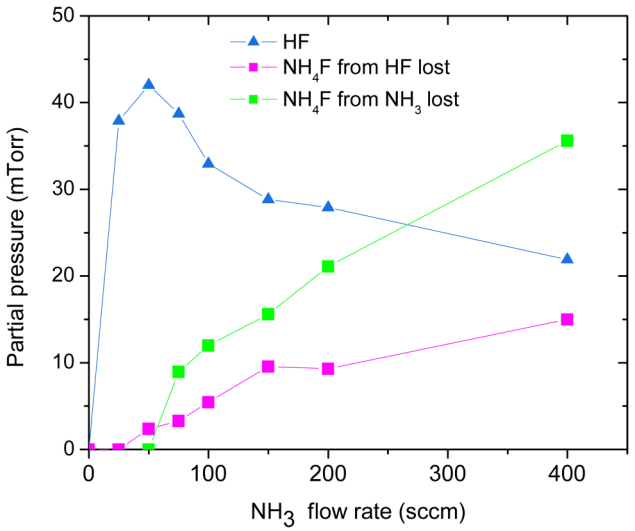

FIG. 10. Variation of the HF density as a function of the NH_3 dilution, under conditions of Fig. 9. The magenta and green curves indicate the density of NH_4F deduced, respectively, from the loss of HF and from the loss of NH_3 (assuming that NH_3 reacts with HF to form NH_4F).

IV. CONCLUSIONS

The chemistry of downstream plasmas used for isotropic etching of Si alloys is investigated by VUV absorption spectroscopy and OES both in NF_3/H_2 and NF_3/NH_3 chemistries. In both cases, VUVAS indicates the formation of large amounts of HF molecules which are expected to play a role in oxide etching. F atoms are shown to react rapidly with H_2 and NH_3 to produce HF until all the fluorine is consumed. Also, H rapidly reacts with NF_2 and NF for producing HF and consuming NF_x radicals, which could not be detected by UVAS in the downstream chamber. In the NF_3/NH_3 chemistry, the HF density is shown to decrease when the NH_3 flow rate is increased above the NF_3 flow rate. This decay scales with the amount of NH_3 that is lost, which is attributed to an efficient reaction between NH_3 and HF to form the NH_4F molecule that is supposed to be the precursor for salt formation on the wafer. Though NH_4F was not directly observed in the plasma, its density could be estimated based on the quantity of HF and the lost NH_3.

ACKNOWLEDGMENTS

This work was partly supported by the LabEx Minos (No. ANR-10-LABX-55-01) and by the French RENATECH network. The authors would like to acknowledge Applied Materials for their technical support.

REFERENCES

[1]S. M. Irving, Solid State Technol. **14**, 47 (1971).
[2]V. M. Donnelly and A. Kornblit, J. Vac. Sci. Technol. A **31**, 050825 (2013).
[3]C. T. Carver, J. Plombon, P. E. Romero, S. Suri, T. A. Tronic, and R. B. Turkot, Jr., ECS J. Solid State Sci. Technol. **4**, N5005 (2015).
[4]J. Jang *et al.*, 2009 Symposium on VLSI Technology, Honolulu, HI, 15–17 June 2009 (IEEE, Honolulu, 2009), p. 192.
[5]E. Prévost, G. Cunge, C. De-Buttet, S. Lagrasta, L. Vallier, and C. Petit-Etienne, Proc. SPIE **10149**, 101490M (2017).
[6]N. Posseme, O. Pollet, and S. Barnola, Appl. Phys. Lett. **105**, 051605 (2014).
[7]E.-J. Song, J.-H. Kim, J.-D. Kwon, S.-H. Kwon, and J.-H. Ahn, Jpn. J. Appl. Phys. **57**, 106505 (2018).
[8]S. Huang, V. Volynets, J. R. Hamilton, S.-K. Nam, I.-C. Song, S. Lu, J. Tennyson, and M. J. Kushner, J. Vac. Sci. Technol. A **36**, 021305 (2018).
[9]B. E. E. Kastenmeier, P. J. Matsuo, G. S. Oehrlein, and J. G. Langan, J. Vac. Sci. Technol. A **16**, 2047 (1998).
[10]H. Nishino, N. Hayasaka, and H. Okano, J. Appl. Phys. **74**, 1345 (1993).
[11]M. T. Suzuki, J. Kikuchi, M. Nagasaka, and S. Fujimura, Mater. Res. Soc. Symp. Proc. **477**, 167 (1997).
[12]W. S. Kim, W. G. Hwang, I. K. Kim, K. Y. Yun, K. M. Lee, and S. K. Chae, Solid State Phenom. **103**, 63 (2005).
[13]Y. Hagimoto, H. Ugajin, D. Miyakoshi, H. Iwamoto, Y. Muraki, and T. Orii, Solid State Phenom. **134**, 7 (2008).
[14]T. Kusuki, H. Kawakami, H. Sakaue, and Y. Horiike, Extended Abstracts of Electrochemical Society Meeting, Honolulu, HI, 16–21 May 1993 (IOPP, Honolulu, 1993), p. 375.
[15]H. Ogawa, T. Arai, M. Yanagisawa, T. Ichiki, and Y. Horiike, Jpn. J. Appl. Phys. **41**, 5349 (2002).
[16]A. J. Sidhwa, F. C. Goh, H. A. Naseem, and W. D. Brown, J. Vac. Sci. Technol. A **11**, 1156 (1993).
[17]K. Shinoda, N. M. H. Kobayashi, M. Izawa, T. Saeki, K. Ishikawa, and M. Hori, J. Vac. Sci. Technol. A. **37**, 051002 (2019).
[18]V. Martirosyan, E. Despiau-Pujo, J. Dubois, G. Cunge, and O. Joubert, J. Vac. Sci. Technol. A **36**, 041301 (2018).
[19]V. Martirosyan, O. Joubert, and E. Despiau-Pujo, J. Phys. D Appl. Phys. **52**, 055204 (2018).
[20]V. Ah-Leung, O. Pollet, N. Possémé, M. Garcia, B. Névine Rochat, C. Guedj, G. Audoit, and S. Barnola, J. Vac. Sci. Technol. A **35**, 021408 (2017).
[21]N. Posseme, V. Ah-Leung, O. Pollet, C. Arvet, and M. Garcia-Barros, J. Vac. Sci. Technol. A **34**, 061301 (2016).
[22]V. Renaud, C. Petit-Etienne, J.-P. Barnes, J. Bisserier, O. Joubert, and E. Pargon, J. Appl. Phys. **126**, 243301 (2019).
[23]A. Tavernier, L. Favennec, T. Chevolleau, and V. Jousseaume, ECS Trans. **45**, 225 (2012).
[24]H. J. Oh, J. H. Lee, M. S. Lee, W. G. Shin, S. Y. Kang, G. D. Kim, and D. H. Ko, ECS Trans. **61**, 1 (2014).
[25]M. A. A. Clyne, D. J. McKenney, and R. F. Walker, Can. J. Chem. **51**, 3596 (1973).
[26]R. F. Heidner, J. F. Bott, C. E. Gardner, and J. E. Melzer, J. Chem. Phys. **70**, 4509 (1979).
[27]K. H. Homann, W. C. Solomon, J. Warnatz, H. G. Wagner, and C. Zetzsch, Ber. Bunsenges. Phys. Chem. **74**, 585 (1970).
[28]E. E. Wurzburg and P. L. Houston, J. Chem. Phys. **72**, 4811 (1980).
[29]J. M. Herbelin and N. Cohen, Chem. Phys. Lett. **20**, 605 (1973).
[30]L. Tian, Y. Zhu, H. Song, and M. Yang, Phys. Chem. Chem. Phys. **21**, 11385 (2019).
[31]G. Cunge, M. Fouchier, M. Brihoum, P. Bodart, M. Touzeau, and N. Sadeghi, J. Phys. D Appl. Phys. **44**, 122001 (2011).
[32]G. Cunge, P. Bodart, M. Brihoum, F. Boulard, T. Chevolleau, and N. Sadeghi, Plasma Sources Sci. Technol. **21**, 4006 (2012).
[33]J. W. Coburn and H. F. Winters, J. Vac. Sci. Technol. **16**, 391 (1979).
[34]V. M. Donnelly and M. J. Schabel, J. Appl. Phys. **91**, 6288 (2002).
[35]J.-P. Booth, O. Joubert, J. Pelletier, and N. Sadeghi, J. Appl. Phys. **69**, 618 (1991).
[36]J.-P. Booth and N. Sadeghi, J. Appl. Phys. **70**, 611 (1991).
[37]J.-P. Booth and G. Cunge, F. Neuilly, and N. Sadeghi, Plasma Sources Sci. Technol. **7**, 423 (1998).
[38]M. Kogelschatz, G. Cunge, and N. Sadeghi, J. Phys. D Appl. Phys. **37**, 1954 (2004).
[39]B. M. Cheng, H. C. Lu, H. K. Chen, M. Bahou, Y. P. Lee, A. M. Mebel, L. C. Lee, M. C. Liang, and Y. L. Yung, Astrophys. J. **647**, 1535 (2006).
[40]J. A. Syage, R. B. Cohen, and J. Steadman, J. Chem. Phys. **97**, 6072 (1992).
[41]V. Vaida, M. I. McCarthy, P. C. Engelking, and P. Botschwina, J. Chem. Phys. **86**, 6669 (1987).
[42]Y. J. Wu, H. C. Lu, H. K. Chen, and B. M. Cheng, J. Chem. Phys. **127**, 154311 (2007).
[43]S. R. La Paglia and A. B. F. Duncan, J. Chem. Phys. **34**, 1003 (1961).
[44]T. Shirafuji and K. Tachibana, Appl. Surf. Sci. **79**, 117 (1994).
[45]V. C. Papadimitriou, M. R. McGillen, E. L. Fleming, C. H. Jackman, and J. B. Burkholder, Geophys. Res. Lett. **40**, 440 (2013).
[46]J. B. Nee, M. Suto, and L. C. Lee, J. Phys. B At. Mol. Phys. **18**, L293 (1985).
[47]F. Carnovale, R. Tseng, and C. E. Brion, J. Phys. B At. Mol. Phys. **14**, 4771 (1981).
[48]K. P. Huber and G. Herzberg, *Molecular Spectra and Molecular Structure Constants of Diatomic Molecules* (van Nostrand-Reinhold, New York, 1979), Vol. IV.
[49]C. T. Cheah, M. A. A. Clyne, and F. D. Whitefield, J. Chem. Soc. Faraday Trans. II **76**, 711 (1980).
[50]C. T. Cheah and M. A. A. Clyne, J. Photochem. **15**, 21 (1981).
[51]J. J. Sloan, D. G. Watson, and J. Williamson, Chem. Phys. Lett. **74**, 481 (1980).
[52]C. Xiao, G. Shen, X. Wang, H. Fan, and X. Yang, J. Phys. Chem. **114**, 4520 (2010).
[53]H. J. Riedl and J. Dahmlos, U.S. patent 3,005,684 (1961).